Organic & Biomolecular Chemistry

ROYAL SOCIETY OF CHEMISTRY

PAPER

View Article Online
View Journal | View Issue

Cite this: *Org. Biomol. Chem.*, 2025, **23**, 8948

Electrochemical *N*-sulfonylation of *in situ* generated indole-based hydrazones and antimicrobial evaluation

Parmjeet Kaur,[a] Anuj Kumar,[b,c] Tashi Palmo,[b,c] Kuljit Singh *[b,c] and Vikas Tyagi *[a]

Received 9th July 2025,
Accepted 9th September 2025

DOI: 10.1039/d5ob01107h

rsc.li/obc

Herein, we report a novel metal-free electrochemical strategy for regioselective *N*-sulfonylation of *in situ* generated indole-based hydrazones using readily available sodium sulfinates. The feasibility of the protocol was demonstrated by employing differently substituted aldehydes, hydrazines, and sodium sulfinates to access *N*-sulfonylated products in up to 81% isolated yield. Furthermore, various control experiments and cyclic voltammetry studies were performed to get valuable mechanistic insights. These studies suggested the formation of indole–phenyldiazenium as an intermediate while ruling out the possibility of any radical formation during this transformation. In addition, the synthesized compounds were tested for antibacterial activity against Gram-positive and Gram-negative pathogens. Among them, compounds **5d**, **5e**, **5l**, and **5q** were found to have strong and selective antibacterial activity against *Staphylococcus aureus*, with **5d** being the most potent (MIC = 6.87 μM), while showing only moderate activity against Gram-negative pathogens. Furthermore, scanning electron microscopy (SEM) analysis revealed that the most promising hit (**5d**) causes significant morphological alterations and exerts its effects by causing considerable cellular damage.

Introduction

Hydrazone formation is a powerful strategy for functionalizing carbonyl compounds, enabling the introduction of diverse functional groups into organic molecules, biomolecules, and polymers.[1] Furthermore, hydrazones are a key class of biologically active compounds with a wide range of medicinal properties, drawing considerable interest from chemists.[2] In particular, numerous indole-based hydrazone derivatives have been developed and systematically studied for their therapeutic potential, including antibacterial, antimalarial, antitumor, antitubercular, anti-inflammatory, anti-breast cancer and MIF-inhibitory activities (Fig. 1).[3] Their broad pharmacological profiles make them promising drug candidates with the potential for enhanced efficacy and reduced toxicity.[4] Hence, synthetic strategies for the synthesis and functionalization of hydrazones have garnered significant attention over the past years.[5]

On the other hand, organosulfones constitute an important class of compounds with broad utility in pharmaceuticals, advanced materials, and synthetic chemistry.[6] They display a wide range of biological activities, including antibacterial and anticancer properties, and are frequently incorporated as key structural units in therapeutic agents (Fig. 1).[7] Furthermore, organosulfones can be synthesized through various methods using sulfonylating agents such as sulfonyl chlorides,[8] sulfonyl hydrazides[9] and sodium sulfinates.[10] Traditional approaches, including the oxidation of sulfides[11] and electrophilic aromatic substitution,[12] often involve strong oxidants,[13] odorous thiols[14] or harsh acidic conditions, limiting functional group compatibility.[15] Modern strategies such as transition-metal-catalyzed couplings,[16] C–H activation,[17] and multi-component reactions with SO_2 surrogates[18] have broadened the synthetic scope but still face challenges like high temperatures, toxic by-products, and limited substrate tolerance. In this context, sodium sulfinates have emerged as highly effective sulfonyl donors owing to their bench stability, ease of synthesis, and compatibility with mild reaction conditions, making them a preferred choice.[19] Interestingly, the integration of organosulfone scaffolds with hydrazones within a single structural unit holds significant promise in the search for new bioactive compounds. The combination of sulfone and hydrazone functionalities in the same structural unit not only offers potential for innovative drug development but also opens new avenues in the design of advanced organic optoelectronic materials.[20] As a result, the sulfonylation of hydrazones has received considerable attention in recent years. In this context, Liu and co-

[a]*Department of Chemistry and Biochemistry, Thapar Institute of Engineering and Technology, Patiala-147004, Punjab, India. E-mail: vikas.tyagi@thapar.edu*
[b]*Infectious Diseases Division, CSIR- Indian Institute of Integrative Medicine, Jammu-180001, India. E-mail: singh.kuljit@iiim.res.in*
[c]*Academy of Scientific and Innovative Research (AcSIR), Ghaziabad-201002, India*

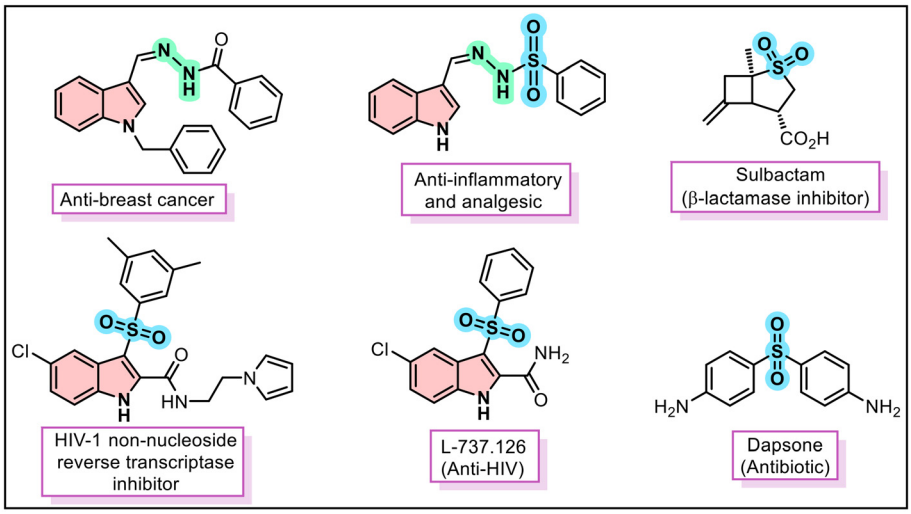

Fig. 1 Pharmacologically relevant indole-based hydrazones and organosulfones.

workers reported an oxidative sulfonylation approach to synthesize β-ketosulfones using a dual-metal co-catalytic system involving copper and silver salts (Scheme 1a).[21] Furthermore, Zhang and colleagues introduced a heterogeneous chitosan@Cu catalyst for C–H sulfonylation of hydrazones by employing sodium sulfinates as sulfonyl donors to access β-ketosulfones (Scheme 1b).[22]

Next, electrochemical synthesis has emerged as a green and sustainable alternative in organic chemistry.[23] It utilizes electricity as a clean reagent, minimizes waste generation, reduces reliance on hazardous chemicals, and typically proceeds under mild conditions, making it an eco-friendly and energy-efficient approach for the synthesis/functionalization of organic molecules like hydrazones.[24] In this context, Hajra *et al.* developed an electrochemical method for the direct C–H sulfonylation of aldehyde hydrazones using sodium sulfinates as sulfonylating agents, leading to the synthesis of various (*E*)-sulfonylated hydrazones (Scheme 1c).[7c] Subsequently, Guo and co-workers reported a related C–H sulfonylation approach employing a range of sodium sulfinates to obtain both alkylated and arylated sulfonylated hydrazones (Scheme 1d).[25] Herein, we aim to develop a novel electrochemical strategy for the regioselective *N*-sulfonylation of *in situ* generated indole-based hydrazones using sodium sulfinates (Scheme 1e). This method offers a sustainable and operationally simple route to access a broad range of clinically important *N*-sulfonylated hydrazones under environmentally benign conditions. Subsequently, the antibacterial efficacy of the newly synthesized molecules against a panel of Gram-positive and Gram-negative pathogens was evaluated.

Results and discussion

To establish the optimal reaction conditions for the one-pot synthesis of compound **5a**, we initiated our study using indole-3-carboxaldehyde **1a**, phenylhydrazine **2a**, and sodium *p*-toluenesulfinate **3a** as the model substrates. The reaction was initially performed in an undivided electrochemical cell using a carbon anode and a nickel cathode under a constant current of 5 mA (entry 1, Table 1). A mixture of ammonium acetate (NH_4OAc) and potassium iodide (KI) served as the supporting electrolyte, with acetonitrile (ACN) as the solvent. Under these conditions, compound **5a** was obtained with 82% conversion (entry 1, Table 1). Subsequent screening of various electrode combinations (entries 2–6, Table 1), while keeping all other reaction parameters unchanged, did not lead to improved yields. When iron and copper were used as cathodes, the product was formed but the starting material (**1a**) was also recovered (entries 5 and 6, Table 1). Furthermore, the reaction provided almost a similar yield when a platinum or nickel electrode was employed as the cathode along with carbon as the anode (entries 1 & 3, Table 1); however, nickel was preferred over platinum owing to its cost-effectiveness, and selected for further optimization. Additionally, when the reaction was carried out in the absence of electricity, only trace amounts of the product (**5a**) were detected after 1 hour (entry 7, Table 1). Next, we examined the impact of the electrolyte on the reaction. In this context, replacing the NH_4OAc/KI combination with single salts such as tetrabutylammonium iodide (TBAI), tetrabutylammonium acetate (TBAOAc), lithium perchlorate ($LiClO_4$) or sodium acetate (NaOAc) resulted in no product formation (entries 8–11, Table 1), suggesting that a synergistic effect of both ammonium acetate and iodide salts is essential. Further investigations showed that when NH_4OAc or KI was used individually, no product (**5a**) was formed (entries 12 and 13, Table 1). However, combining TBAOAc with various halide salts revealed that the reaction proceeded efficiently only with KI (entry 14, Table 1), while the use of KBr or $MgBr_2$ led to significantly lower conversions (entries 15 and 16, Table 1). These observations highlight the important role of iodide and acetate ions in this reaction. Additionally, reactions using TBAI

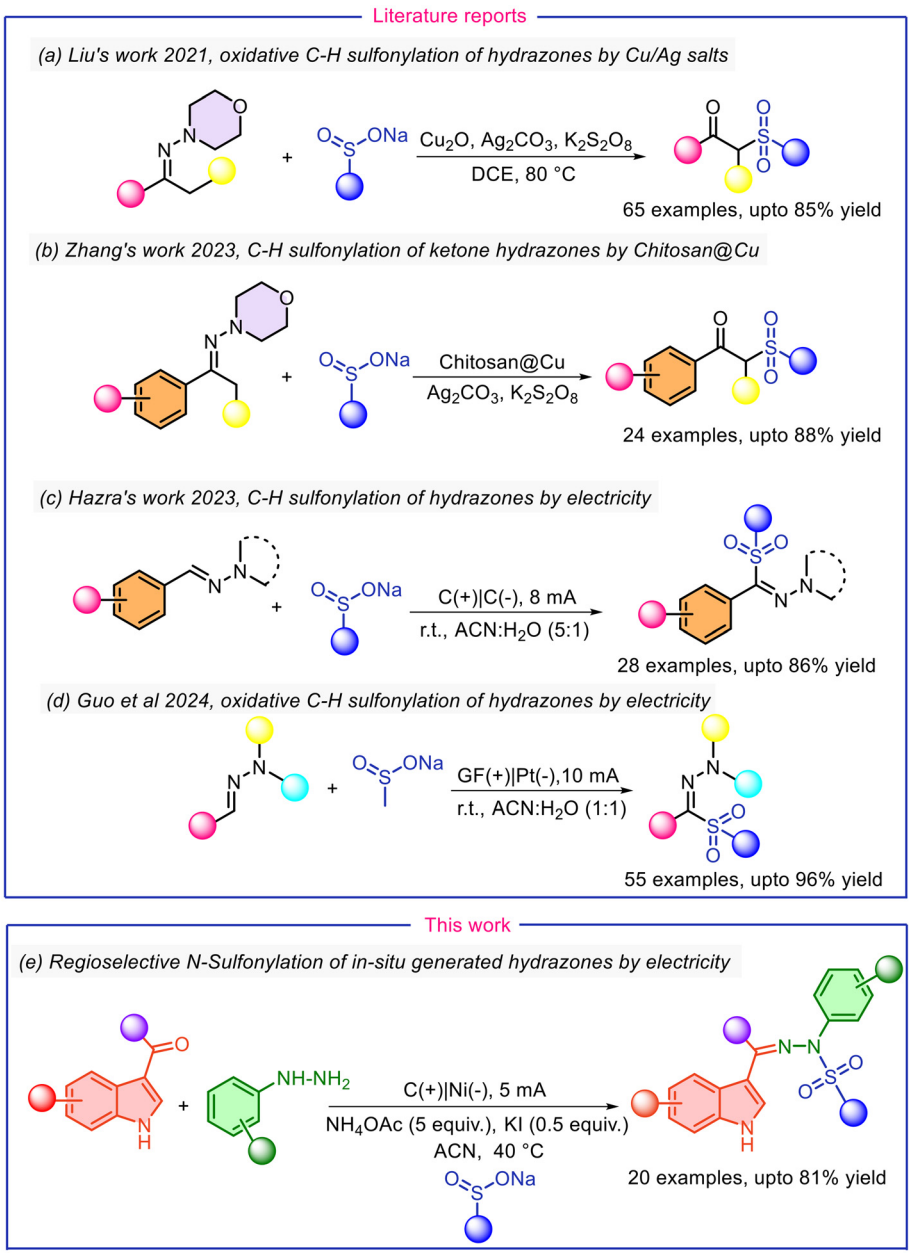

Scheme 1 Recent methods for sulfonylation of hydrazones using sodium sulfinates.

in combination with NH_4OAc also led to successful product formation, further confirming the necessity of both iodide and acetate ions (entry 17, Table 1).

The use of $LiClO_4$ with KI again failed to yield the product, reinforcing the specificity of the required electrolyte system (entry 18, Table 1). Importantly, the use of elemental iodine (I_2) instead of iodide salts resulted in no product formation, further emphasizing the crucial role of the iodide ion (entry 19, Table 1).

Next, solvent screening showed that replacing acetonitrile (ACN) with ACN : H_2O (1 : 1, v/v), ethanol (EtOH), 1,2-dichloroethane (DCE), or DMSO resulted in significantly reduced conversions (entries 20–23, Table 1). In the case of ACN : H_2O (1 : 1, v/v) and EtOH, 22% and 25% conversion of **5a** was observed, respectively, with the recovery of the starting material **1a**. Similarly, the reaction in DCE led to only 5% conversion. In contrast, no conversion was observed in DMSO, and **1a** was recovered unchanged. These findings confirmed that acetonitrile is the optimal solvent for achieving higher product yields. Variation of the applied current also affected the reaction outcome. Reducing the current to 1 mA resulted in a substantial drop in yield, likely due to insufficient conductivity, which prevented the reaction from proceeding efficiently (entry 24, Table 1). Conversely, increasing the current to 10 mA led to partial decomposition of the reactants; however, a moderate 77% conversion to product **5a** was still achieved (entry

Table 1 Optimization of reaction conditions[a]

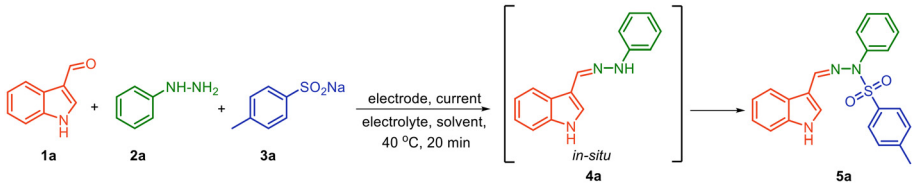

Entry	Electrode	Current	Salts	Equiv. of salts	Solvent	Conversion[b] (%)
1	C(+)|Ni(−)	5 mA	NH_4OAc/KI	5 : 0.5	ACN	82
2	Pt(+)|Pt(−)	5 mA	NH_4OAc/KI	5 : 0.5	ACN	77
3	C(+)|Pt(−)	5 mA	NH_4OAc/KI	5 : 0.5	ACN	79
4	C(+)|C(−)	5 mA	NH_4OAc/KI	5 : 0.5	ACN	70
5	C(+)|Fe(−)	5 mA	NH_4OAc/KI	5 : 0.5	ACN	68
6	C(+)|Cu(−)	5 mA	NH_4OAc/KI	5 : 0.5	ACN	66
7	—	—	NH_4OAc/KI	5 : 0.5	ACN	4
8	C(+)|Ni(−)	5 mA	TBAI	5.0	ACN	0
9	C(+)|Ni(−)	5 mA	TBAOAc	5.0	ACN	0
10	C(+)|Ni(−)	5 mA	$LiClO_4$	5.0	ACN	0
11	C(+)|Ni(−)	5 mA	NaOAc	5.0	ACN	0
12	C(+)|Ni(−)	5 mA	NH_4OAc	5.0	ACN	0
13	C(+)|Ni(−)	5 mA	KI	5.0	ACN	0
14	C(+)|Ni(−)	5 mA	TBAOAc/KI	5 : 0.5	ACN	72
15	C(+)|Ni(−)	5 mA	TBAOAc/KBr	5 : 0.5	ACN	40
16	C(+)|Ni(−)	5 mA	TBAOAc/$MgBr_2$	5 : 0.5	ACN	36
17	C(+)|Ni(−)	5 mA	TBAI/NH_4OAc	5 : 0.5	ACN	73
18	C(+)|Ni(−)	5 mA	$LiClO_4$/KI	5 : 0.5	ACN	0
19	C(+)|Ni(−)	5 mA	I_2	5.0	ACN	0
20	C(+)|Ni(−)	5 mA	NH_4OAc/KI	5 : 0.5	ACN : H_2O (1 : 1, v/v)	22
21	C(+)|Ni(−)	5 mA	NH_4OAc/KI	5 : 0.5	EtOH	25
22	C(+)|Ni(−)	5 mA	NH_4OAc/KI	5 : 0.5	DCE	5
23	C(+)|Ni(−)	5 mA	NH_4OAc/KI	5 : 0.5	DMSO	0
24	C(+)|Ni(−)	1 mA	NH_4OAc/KI	5 : 0.5	ACN	70
25	C(+)|Ni(−)	10 mA	NH_4OAc/KI	5 : 0.5	ACN	77
26	C(+)|Ni(−)	5 mA	NH_4OAc/KI	5 : 0.5	ACN	54[c]
27	C(+)|Ni(−)	5 mA	NH_4OAc/KI	5 : 0.5	ACN	65[d]
28	C(+)|Ni(−)	5 mA	NH_4OAc/KI	5 : 1	ACN	79
29	C(+)|Ni(−)	5 mA	NH_4OAc/KI	3 : 0.5	ACN	63
30	C(+)|Ni(−)	5 mA	NaOAc/KI	5 : 0.5	ACN	67

[a] Reaction conditions: **1a** (10 mg, 0.07 mmol), **2a** (8 μL, 0.08 mmol), **3a** (24 mg, 0.13 mmol), solvent (2 mL) under a constant current flow in an undivided cell with electrodes at 40 °C. [b] Determined by HPLC. [c] Temperature 30 °C. [d] Temperature 50 °C.

25, Table 1). Finally, changing the reaction temperature (entries 26 and 27, Table 1) did not lead to any notable improvement in yield. Next, the ratio of NH_4OAc and KI was varied; however, the reaction gave an inferior yield (entries 28 and 29, Table 1). Moreover, a change in the substrate's molar ratio did not improve the reaction outcome. Notably, using the NaOAc/KI salt combination resulted in a decreased yield of product **5a** (67%) (entry 30, Table 1).

With the best reaction conditions in hand, we explored the substrate scope by employing a range of electronically and structurally diverse aldehydes, sulfinate salts, and hydrazines. Indole-3-carboxaldehydes bearing electron-donating groups afforded higher yields compared to the unsubstituted indole-3-carboxaldehydes (**5a–5c**, Scheme 2). Moreover, indole-3-carboxaldehydes containing halide substituents at the C-4 and C-5 positions gave good yields of the desired products (**5d–5f**, Scheme 2). However, a significant drop in yield was observed when aldehydes containing strong electron-withdrawing groups such as NO_2 and CN were used under the same electrochemical conditions with phenyl hydrazine and sodium tosyl sulfinate (**5g** and **5h**, Scheme 2). On extending the methodology to benzaldehydes, we observed that these compounds showed a marked decline in product yields compared to indole-3-carboxaldehydes (**5i** and **5j**, Scheme 2). Furthermore, phenyl sulfinate salts bearing electron-donating groups or halide substituents gave satisfactory results (**5k–5m**, Scheme 2). In contrast, phenyl sulfinate salts with strong electron-withdrawing groups such as CF_3 and NO_2 led to a considerable decrease in yield, likely due to reduced nucleophilicity of the $PhSO_2^-$ anion (**5n** and **5o**, Scheme 2).[26] When methyl sodium sulfinate ($MeSO_2Na$) was used in place of aryl sulfinates, a noticeable decline in product yield was observed, which may be attributed to the absence of conjugation and reduced nucleophilicity of the sulfonyl sulfur (**5p**, Scheme 2).[27] Furthermore, we tested the reaction with sodium vinylsulfinate; however, no desired sulfonylated product was obtained, indicating that the current protocol is not effective for alkenyl sulfinates (**5q**, Scheme 2). Next, we examined hydrazines

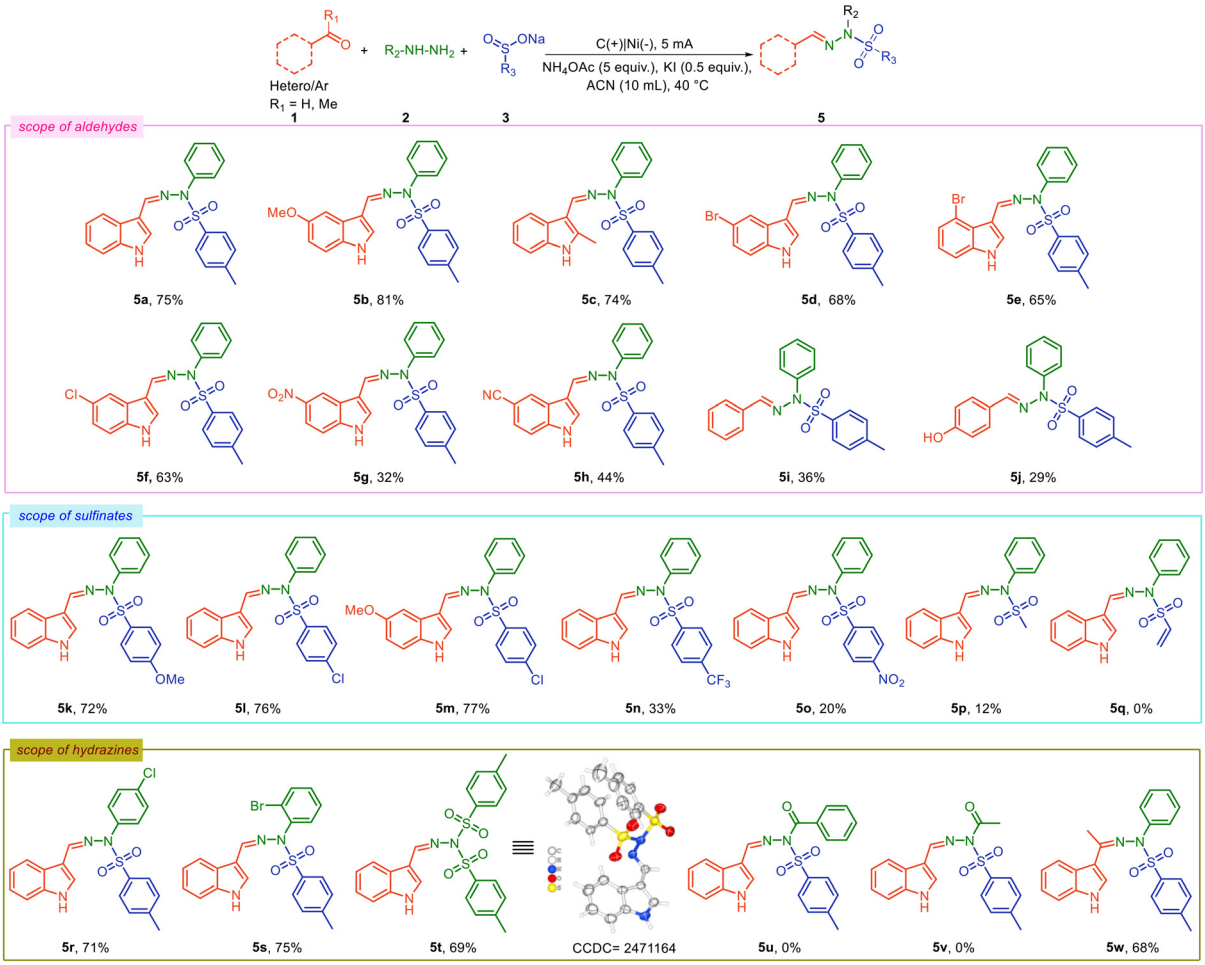

Scheme 2 Substrate scope of electrochemical *N*-sulfonylation of *in situ* generated hydrazones. Reaction conditions: C anode, Ni cathode, aldehydes **1** (100 mg, 0.68 mmol, 1 equiv.), hydrazines **2** (81 μL, 0.82 mmol, 1.2 equiv.), sodium sulfinates **3** (245 mg, 1.37 mmol, 2 equiv.), NH_4OAc (265 mg, 3.4 mmol, 5 equiv.), KI (57 mg, 0.34 mmol, 0.5 equiv.), ACN (10 mL) under a constant current flow of 5 mA in an undivided cell with electrodes at 40 °C, isolated yields.

bearing halide substituents, which also resulted in decreased yields (**5r** and **5s**, Scheme 2). Interestingly, the reaction gave the corresponding product in 69% isolated yield when tosyl hydrazine was employed instead of phenyl hydrazine (**5t**, Scheme 2). When acyl and benzoyl hydrazines were tested, they did not provide the desired sulfonylated products (**5u** and **5v**, Scheme 2). However, when the scope was extended to ketone derivatives such as 3-acetylindole, we were delighted to obtain the corresponding product in 68% yield (**5w**, Scheme 2). Further, there was no reaction when N-methyl indole was employed in the reaction.

A proposed reaction mechanism for the regioselective synthesis of compound **5a** is depicted in Scheme 3. Initially, KI reacts with ACN and undergoes anodic oxidation to generate the iodinium species $[(CH_3CN)_2I^+]$.[28] This electrophilic iodinium species subsequently reacts with the *in situ* generated hydrazone **4a**, which is formed *via* the condensation of **1a** and **2a**. Furthermore, the abstraction of a proton by the acetate ion facilitates the formation of the indole hydrazone iodinium

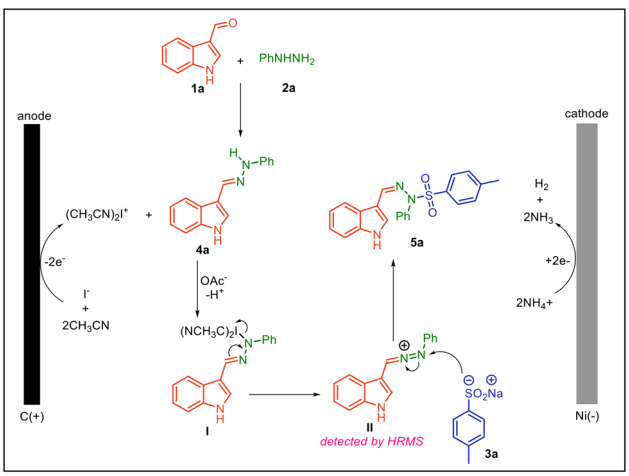

Scheme 3 Plausible mechanism.

intermediate (**I**), which undergoes rearrangement to form indole–phenyldiazenium as an intermediate (**II**) (confirmed using HRMS data, Fig. S2–S4). Thereafter, nucleophilic attack by the sulfinate anion on intermediate (**II**) leads to the formation of the final product **5a**. The use of NH_4OAc in excess is crucial, as it serves not only as a proton abstractor but also undergoes reduction at the cathode during the electrochemical process.[28]

Furthermore, to get more insight into the proposed reaction pathway, a series of control experiments were performed. First, the reaction was conducted in the presence of radical scavengers such as (2,2,6,6-tetramethylpiperidin-1-yl)oxidanyl (TEMPO) (4 equiv.) (Scheme 4a) and butylated hydroxytoluene (BHT) (4 equiv.) (Scheme 4b), and product **5a** was still obtained in good yield under these conditions, thereby ruling out a radical pathway and suggesting that no sulfinate radical intermediate is involved, as reported previously by various groups.[25,29]

Next, cyclic voltammetry studies were carried out to gain more insight into the proposed electrochemical reaction mechanism. In this context, hydrazone **4a** exhibited two distinct oxidation potentials at 0.43 V and 1.78 V (Fig. 2). Separately, KI in acetonitrile showed oxidation waves at 1.00 V and 1.50 V. Interestingly, upon addition of KI to the reaction mixture, the first oxidation potential of hydrazone shifted to a more positive value (0.53 V), indicating the formation of the indole hydrazone iodinium intermediate **I**.[28]

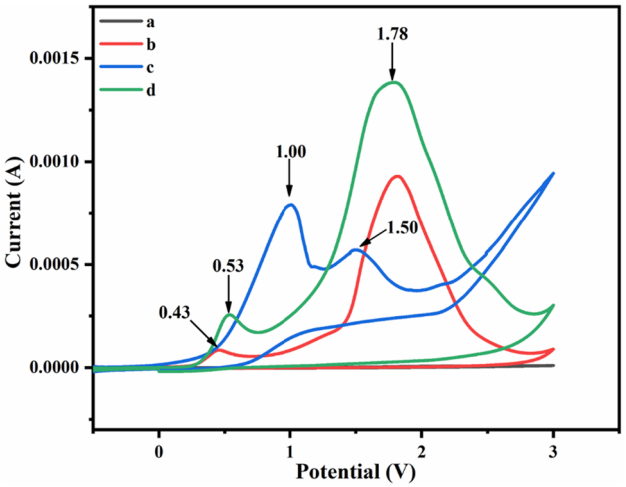

Fig. 2 Cyclic voltammograms (IUPAC convention) recorded in 0.1 M $^nBu_4NPF_6$/ACN at room temperature using a Pt working electrode, a Pt wire counter electrode, and an Ag/AgCl reference electrode. Scan rate: 0.05 V s^{-1}; initial potential: 0 V; scan direction: 0 → +3 V (oxidative). (a) ACN, (b) **4a** (0.001 M), (c) KI (0.024 M), (d) KI (0.024 M) and **4a** (0.001 M).

Antibacterial susceptibility analysis of the synthesized derivatives

Primarily, whole-cell screening of the synthesized derivatives (**5a–5s**) was conducted at a single concentration of 50 μM against Gram-positive and Gram-negative pathogens. This led to the identification of four potent hits, **5d**, **5e**, **5l**, and **5q**, that exhibited a growth inhibition of >85% against the Gram-positive pathogen *S. aureus*. On the other hand, these derivatives showed a moderate inhibitory effect against Gram-negative pathogens. The average percentage viability of the pathogens in the presence of derivatives **5d**, **5e**, **5l**, and **5q** is shown in Table 2. These findings highlight the selective antibacterial potential of the identified molecules toward the Gram-positive pathogen *S. aureus*. Next, the minimum inhibitory concentration (MIC) of the shortlisted hits was determined against *S. aureus* using the broth micro-dilution assay to further assess their antibacterial potency. The active hits were tested at varied concentrations using vancomycin as the positive control in the experimentation. Compounds **5d**, **5e**, **5l**, and **5q** exhibited

Table 2 Percentage viability of *S. aureus*, *K. pneumoniae*, *A. baumannii*, and *E. coli* pathogens at 50 μM concentration of derivatives. The results are expressed as mean ± standard deviation of three independent experiments

Compound code	Percentage viability			
	S. aureus	*K. pneumonia*	*A. baumannii*	*E. coli*
5d	0.24 ± 0.12	84.17 ± 2.31	80.52 ± 1.68	78.59 ± 1.77
5e	10.26 ± 0.87	94.93 ± 2.03	>100	82.79 ± 2.85
5l	0.24 ± 0.11	>100	>100	81.78 ± 2.59
5q	1.73 ± 0.13	73.27 ± 1.46	85.54 ± 2.24	98.15 ± 1.25

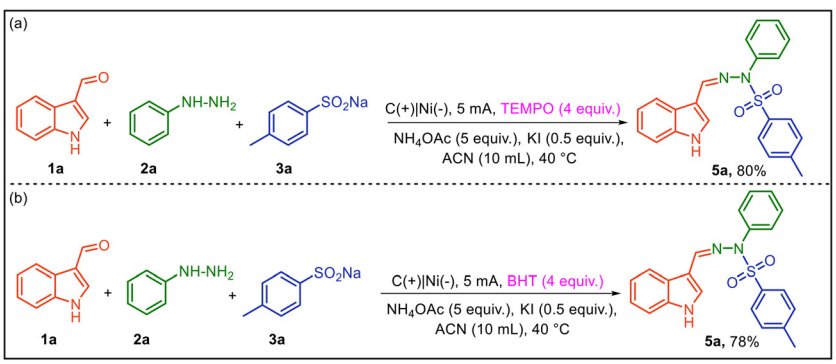

Scheme 4 Radical scavenging experiments.

effective antimicrobial activity against *S. aureus*. Among these hits, compound **5d** emerged as the most potent hit with an MIC value of 6.87 μM. The other three active hits (**5e**, **5l**, and **5q**) displayed MIC values in the range of 10 to 26 μM. The dose–response curves of the four shortlisted hits and the standard drug (vancomycin) are shown in Fig. 3.

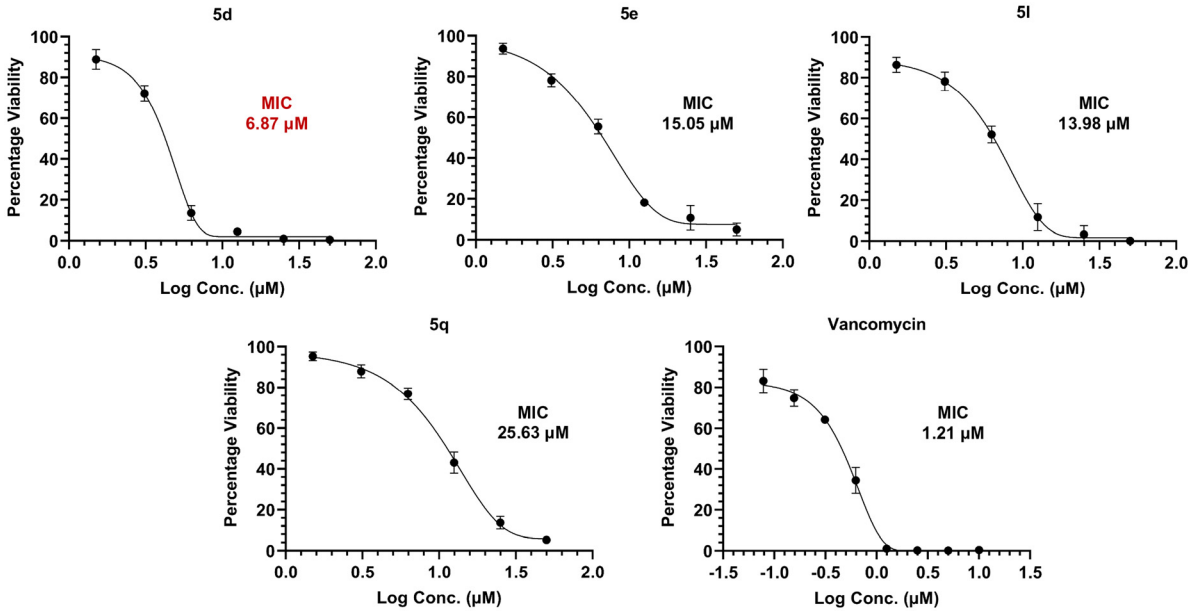

Fig. 3 Dose-dependent curves of the four shortlisted hits against the *S. aureus* pathogen. Vancomycin was used as a standard drug control in the experiment. All the results are presented as mean ± standard deviation of three independent experiments.

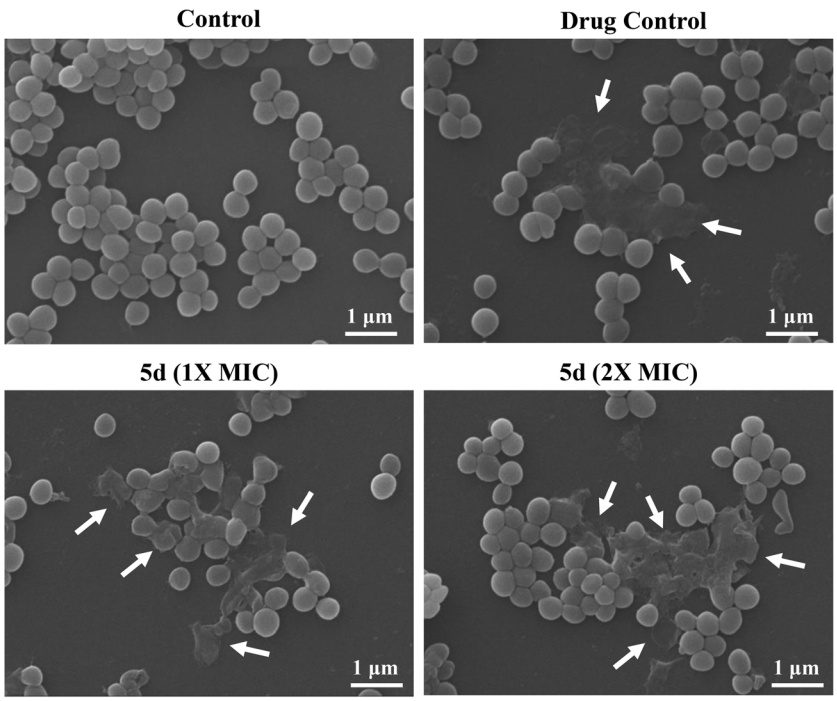

Fig. 4 Scanning electron microscopy (SEM) analysis of *S. aureus* cells. Untreated control and drug control (vancomycin) at 1× MIC. The *S. aureus* pathogen exposed to potent hit (**5d**) at 1× and 2× MIC, respectively. White arrows in the figure depict the damage to the bacterial pathogen after treatment (scale bar = 1 μm).

Scanning electron microscopy (SEM) analysis

The SEM technique was used to visualize the ultrastructural changes in the bacterial cell after treatment with biocidal molecules. Thus, in the present study, we have treated *S. aureus* cells with 1× and 2× MIC of the potent hit **5d** to investigate any structural irregularities and morphological alterations in the bacterial pathogen (Fig. 4). SEM analysis revealed that untreated cells had smooth surfaces with round shapes, whereas cells treated with the control drug at 1× MIC showed considerable damage. Upon treatment with the potent hit **5d** at 1× and 2× MIC, substantial morphological changes, including surface depression and wrinkled and irregular appearance, are visible, leading to bacterial cell death.

Conclusions

In summary, we have developed a novel electrochemical methodology for the regioselective *N*-sulfonylation of *in situ* generated indole-based hydrazones. The scope and robustness of this eco-friendly protocol were demonstrated through the successful transformation of a wide variety of aldehydes, hydrazines, and sodium sulfinates, affording the corresponding *N*-sulfonylated products in good yields. To confirm the essential role of electrical input in this transformation, a series of control experiments were carried out. Furthermore, cyclic voltammetry analyses were conducted to gain mechanistic insights and support the proposed reaction pathway. Next, the synthesized compounds were tested at 50 μM to evaluate their antibacterial activity. Four compounds, **5d**, **5e**, **5l**, and **5q**, stood out by showing strong inhibition (over 85%) against *S. aureus*, a common Gram-positive bacterium. However, they were only moderately effective against Gram-negative bacteria. Further testing confirmed that these hits, especially **5d** with an MIC of 6.87 μM, showed promising and selective activity against *S. aureus*. These findings suggest that the identified compounds could serve as potential leads for developing targeted treatments against Gram-positive infections. Other advanced antimicrobial biological studies are in progress in our lab and will be reported in due course. This study not only underscores the utility of electrochemical synthesis in modern organic chemistry but also opens new avenues for the sustainable development of medicinally important sulfonamide derivatives as antibacterial compounds.

Experimental

General information

All chemicals and solvents were obtained from commercial vendors and used without further purification. All the glass and plasticware utilized in experimentation were sourced from Borosil Scientific (India) and Tarsons (India). Electrochemical reactions were carried out using an OWON (P4305) instrument in an undivided electrochemical cell equipped with a magnetic stirrer. Reaction progress was monitored by thin-layer chromatography (TLC), using silica gel-coated glass plates. Column chromatography was performed using silica gel (60–120 mesh) as the stationary phase, with a solvent system of diethyl ether and hexane serving as the mobile phase. ^{1}H and ^{13}C NMR spectra of the synthesized compounds were recorded on a Bruker spectrometer operating at 700/500/400 MHz and 176/126/101 MHz respectively. Tetramethylsilane (TMS) was used as an internal reference in $CDCl_3$. Chemical shifts (δ) are given in parts per million (ppm), and coupling constants (J) are reported in hertz (Hz). Residual solvent signals were used for calibration: $CDCl_3$ at 7.26 ppm (^{1}H) and 77.16 ppm (^{13}C). The NMR data were annotated using the following abbreviations: s (singlet), brs (broad singlet), d (doublet), t (triplet), q (quartet), dd (doublet of doublet), and m (multiplet). High-resolution mass spectrometry (HRMS) was performed on a Waters QTOF (XEVO G2 XS) mass spectrometer using electrospray ionization in the positive mode (ESI^{+}). Reaction conversions were quantified using high-performance liquid chromatography (HPLC) with 1,3-benzodioxole as an internal standard. The HPLC system consisted of a Shimadzu LC-20AD pump, a CTO-10AS column oven, and a photodiode array (PDA) detector. Cyclic voltammetry was conducted using a DY2300 potentiostat to study the redox behaviour relevant to the electrochemical process. Essential reagents like standard antibiotics and resazurin dye were received from Hi-Media (India). The bacterial strains *Staphylococcus aureus* (ATCC 29213), *Klebsiella pneumoniae* (ATCC 15380), *Acinetobacter baumannii* (ATCC 19606), and *Escherichia coli* (ATCC 25922) were procured from the institutional microbial repository. For culturing bacterial strains, Luria Bertani (LB) broth and LB agar were procured from Hi-Media (India). Bacterial stocks were preserved in cryovials at −80 °C in 30% glycerol to maintain viability. Fluorescence readings were taken using a Tecan Infinite M200-pro multimode plate reader. A centrifuge (Thermo Fisher 5830R) and a shaker incubator (REMI CIS-24-Plus) were utilized during the experimental procedure. All the biological assays were performed in a biosafety cabinet (ESCO AC2-4S1). The SEM study involved the utilization of GelBond film obtained from Lonza (Rockland, USA).

General procedure for the synthesis of compounds (5a–5s)

A mixture of indole-3-carboxaldehyde (100 mg, 0.68 mmol, 1.0 equiv.), phenylhydrazine (81 μL, 0.82 mmol, 1.0 equiv.), and sodium *p*-toluenesulfinate (245 mg, 1.37 mmol, 2.0 equiv.) was dissolved in 10 mL of ACN in a reaction vial. Thereafter, NH_4OAc (265 mg, 3.4 mmol, 5.0 equiv.) and KI (57 mg, 0.34 mmol, 0.5 equiv.) were added to the reaction mixture. Electrolysis was then carried out by applying a constant current of 5 mA using a carbon anode and a nickel cathode, with the reaction mixture maintained at 40 °C in an oil bath. The mixture was stirred under these conditions for 12 h. Upon consumption of the starting materials, as confirmed by TLC, the electric current was turned off, and the solvent was removed under reduced pressure using a rotary evaporator. The resulting crude product was purified by column chromatography to afford the desired compounds.

Antibacterial susceptibility test (single point assay)

The antibacterial susceptibility of the synthesized compounds was determined against Gram-positive (*S. aureus*) and Gram-negative (*K. pneumoniae*, *A. baumannii*, and *E. coli*) pathogens at a single concentration of 50 μM. Briefly, the parent stocks of 20 mM concentration of the compounds were prepared by dissolving them in DMSO. The logarithmic phase of bacterial culture was adjusted to 0.5 McFarland and further diluted to 1 : 100 to obtain a final cell density of 1×10^6 CFU mL^{-1}.[30,31] Subsequently, 100 μL of this freshly prepared bacterial suspension was dispensed into a 96-well flat-bottom plate containing 50 μM of synthesized compounds in triplicate and incubated for 24 h at 37 °C in a shaker incubator. After incubation, 10 μL of freshly prepared resazurin dye (0.04% dissolved in 1× PBS) was added to the culture plate, followed by another hour of incubation at 37 °C. Finally, the Tecan Infinite M200-pro multimode reader was utilized to measure the fluorescence intensity with excitation and emission wavelengths set at 530 nm and 600 nm, respectively, to calculate the cell viability. The percentage viability of bacterial pathogens was calculated for each compound, and the results are presented as mean ± standard deviation of three independent measurements performed in triplicate.

Minimum inhibitory concentration (MIC)

The minimal inhibitory concentration (MIC), defined as the lowest compound concentration with no visible bacterial growth, was determined for the identified hits using a broth microdilution assay in accordance with the guidelines of the Clinical and Laboratory Standards Institute (CLSI).[32,33] Briefly, the compounds were serially diluted at a gradient concentration ranging from 50 μM to 1.56 μM in 96-well flat-bottom plates. Then, 100 μL of bacterial suspension with a cell density of 1×10^6 CFU mL^{-1} was added to each well and incubated for 24 h at 37 °C. Following incubation, resazurin dye was added, and fluorescence was measured using a plate reader (as described above). Finally, the Gompertz equation was used to determine the MIC, and the data were plotted using GraphPad Prism 9 (Version 9.3.1). The experiment for MIC determination was performed in biological triplicates.

Scanning electron microscopy analysis

Scanning electron microscopy (SEM) was performed as reported previously.[31,34] Bacterial cultures of *S. aureus* in the exponential phase were diluted with 1× PBS to an OD_{600} of 0.06 and then treated with 1× and 2× MIC of the potent hit **5d** and incubated at 37 °C for 4 h. Following incubation, bacterial cultures were centrifuged at 5000 rpm for 5 minutes, and the pellet was washed thrice with 1× PBS. After this, 5 μL aliquots of cell suspension were placed onto SEM sheets and left to air dry. Furthermore, the slides were fixed with 4% paraformaldehyde and 2.5% glutaraldehyde and air-dried overnight. After fixation, the slides were immersed in a graded ethanol series (30%, 50%, 70%, 90%, and 100%). The dried samples were coated with colloidal gold using a sputter coater, and morphological changes were examined under a JEOL JSM 6010 PLUS-LA (Akishima, Tokyo, Japan) scanning electron microscope.

Characterization of compounds

(*Z*)-*N*′-((1*H*-Indol-3-yl)methylene)-4-methyl-*N*-phenylbenzenesulfonohydrazide (5a). Off-white solid, ^{1}H NMR (400 MHz, $CDCl_3$): δ 9.26 (brs, 1H), 8.09 (s, 1H), 7.86 (d, J = 8.4 Hz, 2H), 7.71 (s, 1H), 7.50 (d, J = 8.4 Hz, 1H), 7.32 (s, 1H), 7.30 (s, 1H), 7.25 (s, 1H), 7.23 (s, 1H), 7.21 (s, 1H), 7.19 (s, 1H), 7.12 (t, J = 7.6 Hz, 1H), 6.96 (d, J = 7.6 Hz, 1H), 6.91 (d, J = 7.6 Hz, 2H), 2.45 (s, 3H) ppm. ^{13}C NMR (101 MHz, $CDCl_3$): δ 144.2, 142.7, 138.8, 136.4, 136.0, 129.6, 129.3, 128.8, 128.4, 124.6, 123.3, 122.1, 121.5, 119.7, 113.9, 112.5, 21.7 ppm. HRMS (ESI-TOF) m/z: $[M + H]^+$ calcd for $C_{22}H_{20}N_3O_2S$, 390.1276; found, 390.1263.

(*Z*)-*N*′-((5-Methoxy-1*H*-indol-3-yl)methylene)-4-methyl-*N*-phenylbenzenesulfonohydrazide (5b). White solid, ^{1}H NMR (500 MHz, $CDCl_3$): δ 9.02 (brs, 1H), 8.02 (s, 1H), 7.83 (d, J = 8.5 Hz, 2H), 7.60 (d, J = 2.5 Hz, 1H), 7.33 (d, J = 9.0 Hz, 1H), 7.29–7.26 (m, 2H), 7.21–7.18 (m, 2H), 6.92–6.85 (m, 4H), 6.52 (d, J = 2.0 Hz, 1H), 3.63 (s, 3H), 2.42 (s, 3H) ppm. ^{13}C NMR (126 MHz, $CDCl_3$): δ 155.4, 144.2, 142.8, 139.1, 136.4, 129.5, 129.4, 129.0, 128.6, 125.2, 122.1, 113.9, 113.8, 113.3, 101.0, 100.1, 55.8, 21.7 ppm. HRMS (ESI-TOF) m/z: $[M + H]^+$ calcd for $C_{23}H_{22}N_3O_3S$, 420.1381; found, 420.1372.

(*Z*)-4-Methyl-*N*′-((2-methyl-1*H*-indol-3-yl)methylene)-*N*-phenylbenzenesulfonohydrazide (5c). White solid, ^{1}H NMR (500 MHz, $CDCl_3$): δ 8.89 (brs, 1H), 7.89 (s, 1H), 7.75 (d, J = 8.0 Hz, 2H), 7.27 (d, J = 8.0 Hz, 1H), 7.23–7.21 (m, 2H), 7.16–7.13 (m, 2H), 7.09 (m, 1H), 6.97–6.94 (m, 2H), 6.89–6.85 (m, 3H), 2.38 (s, 3H), 2.21 (s, 3H) ppm. ^{13}C NMR (126 MHz, $CDCl_3$): δ 144.0, 142.6, 139.7, 138.5, 137.1, 135.8, 129.5, 129.3, 128.8, 126.4, 122.5, 122.2, 121.1, 118.9, 114.0, 111.2, 97.8, 21.7, 13.2 ppm. HRMS (ESI-TOF) m/z: $[M + H]^+$ calcd for $C_{23}H_{22}N_3O_2S$, 404.1432; found, 404.1422.

(*Z*)-*N*′-((5-Bromo-1*H*-indol-3-yl)methylene)-4-methyl-*N*-phenylbenzenesulfonohydrazide (5d). Off-white solid, ^{1}H NMR (500 MHz, $CDCl_3$): δ 9.43 (brs, 1H), 7.98 (s, 1H), 7.88 (d, J = 8.5 Hz, 2H), 7.62 (d, J = 3.0 Hz, 1H), 7.37 (d, J = 8.5 Hz, 2H), 7.30 (d, J = 3.0 Hz, 2H), 7.26–7.23 (m, 3H), 6.97 (t, J = 7.5 Hz, 1H), 6.89 (d, J = 8.0 Hz, 2H), 2.51 (s, 3H) ppm. ^{13}C NMR (126 MHz, $CDCl_3$): δ 144.6, 142.5, 138.3, 135.8, 134.7, 129.7, 129.4, 129.3, 129.1, 126.4, 126.3, 122.4, 121.9, 114.8, 114.0, 99.4, 21.8 ppm. HRMS (ESI-TOF) m/z: $[M + H]^+$ calcd for $C_{22}H_{19}BrN_3O_2S$, 468.0381; found, 468.0374.

(*Z*)-*N*′-((4-Bromo-1*H*-indol-3-yl)methylene)-4-methyl-*N*-phenylbenzenesulfonohydrazide (5e). Off-white solid, ^{1}H NMR (500 MHz, $CDCl_3$): δ 9.62 (brs, 1H), 7.89 (d, J = 6.5 Hz, 2H), 7.80 (s, 1H), 7.36 (d, J = 2.5 Hz, 1H), 7.33 (dd, J = 7.5, 4.5 Hz, 3H), 7.20–7.15 (m, 3H), 6.96 (t, J = 8.5 Hz, 1H), 6.89 (t, J = 7.5 Hz, 1H), 6.82 (d, J = 8.0 Hz, 2H), 2.45 (s, 3H) ppm. ^{13}C NMR (126 MHz, $CDCl_3$): δ 144.4, 142.6, 138.4, 137.1, 135.8, 129.5, 129.4, 129.3, 129.0, 125.3, 125.1, 124.2, 122.2, 114.1, 113.2, 111.7, 99.0, 21.8 ppm. HRMS (ESI-TOF) m/z: $[M + H]^+$ calcd for $C_{22}H_{19}BrN_3O_2S$, 468.0381; found, 468.0377.

(*Z*)-*N*′-((5-Chloro-1*H*-indol-3-yl)methylene)-4-methyl-*N*-phenylbenzenesulfonohydrazide (5f). Off-white solid, ^{1}H NMR (500 MHz, $CDCl_3$): δ 9.14 (brs, 1H), 7.92 (s, 1H), 7.82 (d, J = 8.5 Hz, 2H), 7.66 (d, J = 3.0 Hz, 1H), 7.36–7.30 (m, 3H), 7.26 (s, 1H), 7.22–7.16 (m, 3H), 7.08 (d, J = 2.0 Hz, 1H), 6.93 (t, J = 7.5 Hz, 1H), 6.87 (d, J = 7.5 Hz, 1H), 2.45 (s, 3H) ppm. ^{13}C NMR (126 MHz, $CDCl_3$): δ 144.5, 142.6, 138.2, 136.0, 134.3, 129.6, 129.5, 129.4, 129.0, 127.4, 125.8, 123.9, 122.4, 119.0, 114.0, 113.4, 21.8 ppm. HRMS (ESI-TOF) m/z: $[M + H]^+$ calcd for $C_{22}H_{19}ClN_3O_2S$, 424.0886; found, 424.0883.

(*Z*)-4-Methyl-*N*′-((5-nitro-1*H*-indol-3-yl)methylene)-*N*-phenylbenzenesulfonohydrazide (5g). Yellow solid, ^{1}H NMR (500 MHz, $CDCl_3$): δ 9.69 (brs, 1H), 8.07–8.04 (m, 2H), 7.92 (s, 1H), 7.85 (d, J = 8.0 Hz, 2H), 7.76 (d, J = 2.0 Hz, 1H), 7.48 (d, J = 9.0 Hz, 1H), 7.34 (d, J = 8.0 Hz, 2H), 7.26 (s, 1H), 7.21–7.18 (m, 2H), 6.98–6.93 (m, 1H), 6.83 (d, J = 7.5 Hz, 1H), 2.46 (s, 3H) ppm. ^{13}C NMR (126 MHz, $CDCl_3$): δ 138.9, 135.4, 131.4, 129.8, 129.5, 129.4, 129.1, 124.5, 122.8, 118.9, 116.5, 114.1, 112.6, 102.4, 21.8 ppm. HRMS (ESI-TOF) m/z: $[M + H]^+$ calcd for $C_{22}H_{19}N_4O_4S$, 435.1127; found, 435.1119.

(*Z*)-*N*′-((5-Cyano-1*H*-indol-3-yl)methylene)-4-methyl-*N*-phenylbenzenesulfonohydrazide (5h). Yellow solid, ^{1}H NMR (500 MHz, $CDCl_3$): δ 9.56 (brs, 1H), 7.87 (s, 1H), 7.83 (d, J = 8.0 Hz, 2H), 7.73 (s, 1H), 7.49–7.46 (m, 3H), 7.42 (d, J = 8.5 Hz, 1H), 7.34 (d, J = 8.0 Hz, 2H), 7.22–7.19 (m, 2H), 6.95 (t, J = 7.5 Hz, 1H), 6.84 (d, J = 8.0 Hz, 1H), 2.47 (s, 3H) ppm. ^{13}C NMR (126 MHz, $CDCl_3$): δ 144.9, 142.3, 137.4, 135.6, 130.5, 129.8, 129.5, 129.1, 126.3, 124.9, 122.8, 119.7, 114.0, 113.5, 105.0, 101.0, 21.8 ppm. HRMS (ESI-TOF) m/z: $[M + H]^+$ calcd for $C_{23}H_{19}N_4O_2S$, 415.1228; found, 415.1223.

(*E*)-*N*′-Benzylidene-4-methyl-*N*-phenylbenzenesulfonohydrazide (5i). Yellow viscous solid, ^{1}H NMR (500 MHz, $CDCl_3$): δ 7.50 (d, J = 2.0 Hz, 1H), 7.48 (t, J = 2.0 Hz, 1H), 7.24 (s, 1H), 7.20 (d, J = 2.0 Hz, 1H), 7.19 (d, J = 2.0 Hz, 1H), 7.15 (d, J = 1.0 Hz, 1H), 7.14 (d, J = 2.0 Hz, 1H), 7.00–6.99 (m, 1H), 6.97 (s, 1H), 6.93 (t, J = 7.5 Hz, 1H), 6.83 (s, 1H), 6.82 (s, 1H), 6.80 (s, 1H), 6.78 (s, 1H), 6.74 (q, J = 4.0 Hz, 4.5 Hz, 1H), 2.24 (s, 3H) ppm. ^{13}C NMR (126 MHz, $CDCl_3$): δ 145.4, 144.8, 135.9, 134.0, 132.8, 132.4, 129.3, 129.1, 129.0, 128.6, 128.5, 128.3, 128.0, 127.9, 127.7, 126.7, 123.8, 122.7, 120.7, 112.8, 70.3, 21.6 ppm. HRMS (ESI-TOF) m/z: $[M + Na]^+$ calcd for $C_{20}H_{18}N_2NaO_2S$, 373.0986; found, 373.0978.

(*E*)-*N*′-(4-Hydroxybenzylidene)-4-methyl-*N*-phenylbenzenesulfonohydrazide (5j). Yellow viscous solid, ^{1}H NMR (500 MHz, $CDCl_3$): δ 7.84 (s, 1H), 7.79 (d, J = 8.0 Hz, 2H), 7.33 (d, J = 7.5 Hz, 2H), 7.26 (s, 1H), 7.22–7.18 (m, 3H), 6.94–6.91 (m, 3H), 6.88 (d, J = 9.0 Hz, 2H), 2.46 (s, 3H) ppm. ^{13}C NMR (126 MHz, $CDCl_3$): δ 158.3, 144.5, 142.9, 142.5, 136.0, 131.7, 129.7, 129.4, 129.1, 122.4, 117.4, 117.0, 113.9, 21.8 ppm. HRMS (ESI-TOF) m/z: $[M + H]^+$ calcd for $C_{20}H_{19}N_2O_3S$, 367.1116; found, 367.1111.

(*Z*)-*N*′-((1*H*-Indol-3-yl)methylene)-4-methoxy-*N*-phenylbenzenesulfonohydrazide (5k). White solid, ^{1}H NMR (500 MHz, $CDCl_3$): δ 9.22 (brs, 1H), 8.03 (s, 1H), 7.86 (d, J = 9.0 Hz, 2H), 7.66 (d, J = 3.0 Hz, 1H), 7.45 (d, J = 8.0 Hz, 1H), 7.22–7.16 (m, 4H), 7.08 (t, J = 8.0 Hz, 1H), 6.93 (d, J = 9.0 Hz, 2H), 6.90 (s, 1H), 6.87 (d, J = 7.5 Hz, 2H), 3.84 (s, 3H) ppm. ^{13}C NMR (126 MHz, $CDCl_3$): δ 163.6, 142.8, 139.1, 136.0, 131.0, 130.7, 129.3, 128.4, 124.6, 123.3, 122.1, 121.5, 119.7, 114.2, 113.8, 112.5, 100.3, 55.7 ppm. HRMS (ESI-TOF) m/z: $[M + H]^+$ calcd for $C_{22}H_{20}N_3O_3S$, 406.1225; found, 406.1219.

(*Z*)-*N*′-((1*H*-Indol-3-yl)methylene)-4-chloro-*N*-phenylbenzenesulfonohydrazide (5l). Off-white solid, ^{1}H NMR (500 MHz, $CDCl_3$): δ 9.15 (brs, 1H), 8.10 (s, 1H), 7.88 (d, J = 8.5 Hz, 2H), 7.70 (s, 1H), 7.49–7.45 (m, 3H), 7.27–7.20 (m, 3H), 7.17–7.10 (m, 2H), 6.94 (t, J = 7.5 Hz, 1H), 6.88 (d, J = 7.5 Hz, 2H) ppm. ^{13}C NMR (126 MHz, $CDCl_3$): δ 142.5, 140.0, 138.2, 138.0, 135.9, 130.2, 129.4, 129.2, 128.5, 124.5, 123.5, 122.4, 121.7, 119.6, 113.9, 112.6, 100.0 ppm. HRMS (ESI-TOF) m/z: $[M + H]^+$ calcd for $C_{21}H_{17}ClN_3O_2S$, 410.0730; found, 410.0720.

(*Z*)-4-Chloro-*N*′-((5-methoxy-1*H*-indol-3-yl)methylene)-*N*-phenylbenzenesulfonohydrazide (5m). Brown solid, ^{1}H NMR (500 MHz, $CDCl_3$): δ 8.98 (brs, 1H), 8.07 (s, 1H), 7.88 (d, J = 9.0 Hz, 2H), 7.64 (d, J = 2.5 Hz, 1H), 7.46 (d, J = 8.5 Hz, 2H), 7.35 (d, J = 8.5 Hz, 1H), 7.23–7.20 (m, 2H), 6.93 (t, J = 7.0 Hz, 1H), 6.88 (d, J = 7.5 Hz, 3H), 6.51 (s, 1H), 3.65 (s, 3H) ppm. ^{13}C NMR (126 MHz, $CDCl_3$): δ 155.5, 142.6, 140.0, 138.5, 138.0, 130.8, 130.4, 129.4, 129.2, 128.6, 125.1, 122.4, 114.0, 113.8, 113.3, 100.9, 99.8, 55.9 ppm. HRMS (ESI-TOF) m/z: $[M + H]^+$ calcd for $C_{22}H_{19}ClN_3O_3S$, 440.0835; found, 440.0826.

(*Z*)-*N*′-((1*H*-Indol-3-yl)methylene)-*N*-phenyl-4-(trifluoromethyl) benzenesulfonohydrazide (5n). Light brown solid, ^{1}H NMR (500 MHz, $CDCl_3$): δ 9.33 (s, 1H), 8.16 (s, 1H), 8.08 (d, J = 8.5 Hz, 2H), 7.75 (d, $^3J_{H-F}$ = 8.5 Hz, 2H), 7.70 (d, J = 2.5 Hz, 1H), 7.47 (d, J = 8.5 Hz, 1H), 7.26–7.18 (m, 3H), 7.14–7.09 (m, 2H), 6.94 (t, J = 7.5 Hz, 1H), 6.83 (d, J = 7.5 Hz, 2H) ppm. ^{13}C NMR (126 MHz, $CDCl_3$): δ 143.2, 142.4, 137.9, 136.0, 129.4, 129.4, 126.0, 124.4, 123.6, 122.6, 121.8, 119.5, 113.9, 112.7, 99.7 ppm. HRMS (ESI-TOF) m/z: $[M + H]^+$ calcd for $C_{22}H_{17}F_3N_3O_2S$, 444.0993; found, 444.0972.

(*Z*)-*N*′-((1*H*-Indol-3-yl)methylene)-4-nitro-*N*-phenylbenzenesulfonohydrazide (5o). Yellow solid, ^{1}H NMR (500 MHz, $CDCl_3$): δ 9.07 (brs, 1H), 8.30–8.27 (m, 2H), 8.20 (s, 1H), 8.11–8.08 (m, 2H), 7.76 (d, J = 2.5 Hz, 1H), 7.50 (d, J = 8.0 Hz, 1H), 7.29–7.27 (m, 1H), 7.24–7.20 (m, 2H), 7.12–7.10 (m, 2H), 6.96 (t, J = 7.5 Hz, 1H), 6.89 (d, J = 8.0 Hz, 2H) ppm. ^{13}C NMR (126 MHz, $CDCl_3$): δ 150.5, 145.8, 142.2, 137.3, 135.9, 129.9, 129.5, 128.7, 124.3, 124.1, 123.8, 122.9, 122.0, 119.5, 114.1, 112.7, 99.9 ppm. HRMS (ESI-TOF) m/z: $[M + H]^+$ calcd for $C_{21}H_{17}N_4O_4S$, 421.0970; found, 421.0959 ppm.

(*Z*)-*N*′-((1*H*-Indol-3-yl)methylene)-*N*-phenylmethanesulfonohydrazide (5p). White solid, ^{1}H NMR (500 MHz, $CDCl_3$): δ 9.10 (brs, 1H), 8.06 (s, 1H), 7.65 (d, J = 2.5 Hz, 1H), 7.42 (d, J = 8.0 Hz, 1H), 7.37 (d, J = 8.0 Hz, 1H), 7.26–7.22 (m, 3H), 7.15 (t, J = 8.0 Hz, 1H), 7.00 (d, J = 8.0 Hz, 2H), 6.93 (t, J = 7.5 Hz, 1H), 3.24 (s, 3H) ppm. ^{13}C NMR (126 MHz, $CDCl_3$): δ 142.7, 138.9, 136.1, 129.5, 128.4, 124.5, 123.6, 122.3, 121.8, 119.8, 113.8, 112.6, 98.9, 40.0 ppm. HRMS (ESI-TOF) m/z: $[M + H]^+$ calcd for $C_{16}H_{16}N_3O_2S$, 314.0963; found, 314.0959 ppm.

(*Z*)-*N*′-((1*H*-Indol-3-yl)methylene)-*N*-(4-chlorophenyl)-4-methylbenzenesulfonohydrazide (5r). Brown solid, ^{1}H NMR (500 MHz, $CDCl_3$): δ 9.21 (brs, 1H), 8.01 (s, 1H), 7.81 (d, J = 8.5 Hz, 2H),

7.67 (d, J = 2.5 Hz, 1H), 7.45 (d, J = 8.0 Hz, 1H), 7.28–7.26 (m, 2H), 7.22 (t, J = 7.0 Hz, 1H), 7.15–7.12 (m, 3H), 7.01 (t, J = 6.0 Hz, 1H), 6.78 (dt, J = 8.5, 3.0 Hz, 2H), 2.41 (s, 3H) ppm. ^{13}C NMR (126 MHz, $CDCl_3$): δ 144.4, 141.4, 139.7, 136.2, 135.9, 129.6, 129.3, 128.9, 128.5, 126.9, 124.5, 123.5, 121.7, 119.6, 115.0, 112.6, 100.1, 21.8. ppm. HRMS (ESI-TOF) m/z: $[M + H]^+$ calcd for $C_{22}H_{19}ClN_3O_2S$, 424.0886; found, 424.0860 ppm.

(*Z*)-*N*′-((1*H*-Indol-3-yl)methylene)-*N*-(2-bromophenyl)-4-methylbenzenesulfonohydrazide (5s). Brown solid, ^{1}H NMR (500 MHz, $CDCl_3$): δ 9.02 (s, 1H), 8.51 (s, 1H), 7.83 (s, 1H), 7.82 (s, 1H), 7.80 (d, J = 2.0 Hz, 2H), 7.48 (d, J = 8.0 Hz, 1H), 7.33 (d, J = 1.5 Hz, 1H), 7.32–7.31 (m, 2H), 7.30 (s, 1H), 7.28 (s, 1H), 7.21 (s, 1H), 7.13 (t, J = 7.5 Hz, 1H), 6.78 (t, J = 7.5 Hz, 1H), 2.41 (s, 3H) ppm. ^{13}C NMR (126 MHz, $CDCl_3$): δ 144.3, 143.7, 141.3, 140.0, 139.2, 136.2, 132.4, 129.8, 129.6, 128.9, 128.6, 128.4, 126.5, 123.5, 122.5, 121.5, 120.6, 115.3, 112.3, 108.2, 100.4, 21.7 ppm. HRMS (ESI-TOF) m/z: $[M + H]^+$ calcd for $C_{22}H_{19}BrN_3O_2S$, 468.0381; found, 468.0367 ppm.

(*Z*)-*N*′-((1*H*-Indol-3-yl)methylene)-4-methyl-*N*-tosylbenzenesulfonohydrazide (5t). Light yellow solid, ^{1}H NMR (700 MHz, $CDCl_3$): δ 9.06 (brs, 1H), 8.62 (s, 1H), 7.99 (d, J = 7.7 Hz, 1H), 7.62 (d, J = 8.4 Hz, 4H), 7.47 (d, J = 9.1 Hz, 2H), 7.32 (t, J = 7.0 Hz, 1H), 7.23 (t, J = 7.7 Hz, 1H), 7.13 (d, J = 8.4 Hz, 4H), 2.42 (s, 6H) ppm. ^{13}C NMR (176 MHz, $CDCl_3$): δ 168.9, 144.9, 137.0, 134.0, 133.7, 129.4, 129.1, 124.6, 124.3, 122.7, 122.4, 112.1, 21.8 ppm. HRMS (ESI-TOF) m/z: $[M + H]^+$ calcd for $C_{23}H_{22}N_3O_4S_2$, 468.1051; found, 468.1051 ppm.

(*Z*)-*N*′-(1-(1*H*-Indol-3-yl)ethylidene)-4-methyl-*N*-phenylbenzenesulfonohydrazide (5w). Brown solid, ^{1}H NMR (500 MHz, $CDCl_3$): δ 9.08 (brs, 1H), 8.39–8.36 (m, 2H), 7.83 (d, J = 3.0 Hz, 2H), 7.42–7.37 (m, 3H), 7.32–7.25 (m, 6H), 7.12–7.10 (m, 1H), 2.53 (s, 6H). ^{13}C NMR (126 MHz, $CDCl_3$): 193.9, 136.6, 131.9, 125.5, 123.8, 122.8, 122.4, 118.6, 111.6, 29.8, 27.7 ppm. HRMS (ESI-TOF) m/z: $[M + H]^+$ calcd for $C_{23}H_{22}N_3O_2S$, 404.1432; found, 404.1428 ppm.

Author contributions

All the designing and syntheses of derivatives, characterization, and preparation of the manuscript were done by P. K. and V. T. All the antibacterial evaluation of the synthesized derivatives was done by A. K., T. P., and K. S.

Conflicts of interest

There are no conflicts of interest associated with this work.

Data availability

The data supporting this article have been included as part of the SI. Supplementary information is available. See DOI: https://doi.org/10.1039/d5ob01107h.

CCDC 2471164 (**5s**) contains the supplementary crystallographic data for this paper.[35]

Acknowledgements

The authors gratefully acknowledge the Thapar Institute of Engineering and Technology – Virginia Tech-Center of Excellence in Emerging Materials, India (TIET/CEEMS/Regular/2022/042) and the DST-INSPIRE Fellowship (DST/INSPIRE Fellowship/2019/IF190908) for financial support. HRMS data were obtained through support from the DST-FIST Grant (SR/FST/CS-II/2018/69) to the Department of Chemistry and Biochemistry, TIET Patiala. Additionally, the authors are thankful to the Department of Chemistry, Panjab University, Chandigarh, for providing access to the Single Crystal X-ray Diffraction (SCXRD) facility for X-ray crystallographic analysis. Anuj Kumar (UGC-SRF) and Tashi Palmo (UGC-JRF) are very thankful to the University Grants Commission (UGC), New Delhi, for their fellowship assistance.

References

1 (*a*) D. K. Patel, K. N. Chaudhary, C. K. Joshi, H. R. Chaudhary, N. S. Panchal, D. D. Patel and D. M. Patel, *Russ. J. Org. Chem.*, 2024, **60**, S213–S222; (*b*) A. Claraz, *Beilstein J. Org. Chem.*, 2024, **20**, 1988–2004; (*c*) A. Ali, M. Khalid, S. Abid, J. Iqbal, M. N. Tahir, A. Rauf Raza, J. Zukerman-Schpector and M. W. Paixão, *Appl. Organomet. Chem.*, 2020, **34**, e5399; (*d*) B. Shao and I. Aprahamian, *Chem*, 2020, **6**, 2162–2173.

2 (*a*) S. Rollas and Ş. Güniz Küçükgüzel, *Molecules*, 2007, **12**, 1910–1939; (*b*) J. D. Rajput, S. D. Bagul and R. S. Bendre, *Res. Chem. Intermed.*, 2017, **43**, 6601–6616; (*c*) M. Khan, G. Ahad, A. Alam, S. Ullah, A. Khan, Kanwal, U. Salar, A. Wadood, A. Ajmal, K. M. Khan, S. Perveen, J. Uddin and A. Al-Harrasi, *Heliyon*, 2024, **10**, e23323; (*d*) S. Boudiba, A. N. Tamfu, K. Hanini, I. Selatnia, L. Boudiba, I. Saouli, P. Mosset, O. Ceylan, D. A. M. Egbe, A. Sid and R. M. Dinica, *J. Chem. Res.*, 2023, **47**, 17475198231184603; (*e*) M.İ Han and N. İmamoğlu, *ACS Omega*, 2023, **8**, 9198–9211; (*f*) Y. Demir, F. S. Tokalı, E. Kalay, C. Türkeş, P. Tokalı, O. N. Aslan, K. Şendil and Ş. Beydemir, *Mol. Divers.*, 2023, **27**, 1713–1733.

3 (*a*) S. Verma, S. Lal, R. Narang and K. Sudhakar, *ChemMedChem*, 2023, **18**, e202200571; (*b*) R. Sreenivasulu, P. Sujitha, S. S. Jadav, M. J. Ahsan, C. G. Kumar and R. R. Raju, *Monatsh. Chem.*, 2017, **148**, 305–314; (*c*) G. Verma, A. Marella, M. Shaquiquzzaman, M. Akhtar, M. R. Ali and M. M. Alam, *J. Pharm. BioAllied Sci.*, 2014, **6**, 69–80; (*d*) S. M. Sondhi, M. Dinodia and A. Kumar, *Bioorg. Med. Chem.*, 2006, **14**, 4657–4663; (*e*) S. Keskin, Ş.D Doğan, M. G. Gündüz, I. Aleksic, S. Vojnovic, J. Lazic and J. Nikodinovic-Runic, *J. Mol. Struct.*, 2022, **1270**, 133936; (*f*) U. Farooq, F. Khan, S. N. Mali, U. Ghaffar, J. Hussain, A. Khan, S. Y. Chaudhari, H. A. Al-Shwaiman, A. M. Elgorban, R. D. Jawarkar, W. U. Islam, A. Al-Harrasi and Z. Shafiq, *RSC Adv.*, 2025, **15**, 13284–13299.

4 J. Wahbeh and S. Milkowski, *SLAS Technol.*, 2019, **24**, 161–168.
5 (*a*) X. Xu, J. Zhang, H. Xia and J. Wu, *Org. Biomol. Chem.*, 2018, **16**, 1227–1241; (*b*) X. Zhang, P. Sivaguru, Y. Pan, N. Wang, W. Zhang and X. Bi, *Chem. Rev.*, 2025, **125**, 1049–1190; (*c*) P. Xu, W. Li, J. Xie and C. Zhu, *Acc. Chem. Res.*, 2018, **51**, 484–495; (*d*) A. Prieto, D. Bouyssi and N. Monteiro, *Eur. J. Org. Chem.*, 2018, 2378–2393.
6 (*a*) M. Jamshidi, A. Amani, S. Khazalpour, S. Torabi and D. Nematollahi, *New J. Chem.*, 2021, **45**, 18246–18267; (*b*) J. P. Colomer, M. Traverssi and G. Oksdath-Mansilla, *J. Flow Chem.*, 2020, **10**, 123–138.
7 (*a*) K. L. Manasa, S. Pujitha, A. Sethi, A. Mohammed, M. Alvala, A. Angeli and C. T. Supuran, *Metabolites*, 2020, **10**, 136; (*b*) Q. Yan, W. Cui, X. Song, G. Xu, M. Jiang, K. Sun, J. Lv and D. Yang, *Org. Lett.*, 2021, **23**, 3663–3668; (*c*) B. Sarkar, P. Ghosh and A. Hajra, *Org. Lett.*, 2023, **25**, 3440–3444; (*d*) S. Yu, J. T. Yu and C. Pan, *Org. Biomol. Chem.*, 2024, **22**, 7753–7766.
8 (*a*) M. Yu, S. Lin, S. Zhang, X. Lin and X. Huang, *Org. Chem. Front.*, 2024, **11**, 4284–4289; (*b*) R. Sridhar, B. Srinivas, V. P. Kumar, M. Narender and K. R. Rao, *Adv. Synth. Catal.*, 2007, **349**, 1873–1876.
9 (*a*) S. Noda and S. Tanimori, *Tetrahedron Green Chem.*, 2023, **1**, 100001; (*b*) C. Huang, C. Kang, H. J. Liu, C. L. Wang, S. Tang, Y. S. Qin, Z. Wei and H. Cai, *Green Chem.*, 2024, **26**, 8706–8710.
10 (*a*) D. Hu, L. Shen, S. S. H. Chaw, K. Liang and C. Xia, *Org. Chem. Front.*, 2024, **11**, 3497–3502; (*b*) T. C. Johnson, B. L. Elbert, A. J. M. Farley, T. W. Gorman, C. Genicot, B. Lallemand, P. Pasau, J. Flasz, J. L. Castro, M. Maccoss, D. J. Dixon, R. S. Paton, C. J. Schofield, M. D. Smith and M. C. Willis, *Chem. Sci.*, 2018, **9**, 629–633.
11 (*a*) R. V. Kupwade, *J. Chem. Rev.*, 2019, **1**, 99–113; (*b*) S. K. R. Parumala and R. K. Peddinti, *Tetrahedron Lett.*, 2016, **57**, 1232–1235.
12 P. Bourbon, E. Appert, A. Martin-Mingot, B. Michelet and S. Thibaudeau, *Org. Lett.*, 2021, **23**, 4115–4120.
13 H. Yu and Y. Zhang, *Chin. J. Chem.*, 2016, **34**, 359–362.
14 G. Laudadio, E. Barmpoutsis, C. Schotten, L. Struik, S. Govaerts, D. L. Browne and T. Noël, *J. Am. Chem. Soc.*, 2019, **141**, 5664–5668.
15 D. Q. Dong, Q. Q. Han, S. H. Yang, J. C. Song, N. Li, Z. L. Wang and X. M. Xu, *ChemistrySelect*, 2020, **5**, 13103–13134.
16 (*a*) Y. Hou, Q. Shen, L. Zhu, Y. Han, Y. Zhao, M. Qin and P. Gong, *RSC Adv.*, 2017, **7**, 50372–50377; (*b*) B. Yang, C. Lian, G. Yue, D. Liu, L. Wei, Y. Ding, X. Zheng, K. Lu, D. Qiu and X. Zhao, *Org. Biomol. Chem.*, 2018, **16**, 8150–8154; (*c*) X. Tang, L. Huang, C. Qi, X. Wu, W. Wu and H. Jiang, *Chem. Commun.*, 2013, **49**, 6102–6104.
17 G. Qiu, K. Zhou and J. Wu, *Chem. Commun.*, 2018, **54**, 12561–12569.
18 (*a*) Y. Chen, P. R. D. Murray, A. T. Davies and M. C. Willis, *J. Am. Chem. Soc.*, 2018, **140**, 8781–8787; (*b*) Z. Lin, L. Huang and G. Yuan, *Chem. Commun.*, 2021, **57**, 3579–3582.
19 (*a*) R. J. Reddy and A. H. Kumari, *RSC Adv.*, 2021, **11**, 9130–9221; (*b*) L. Fu, X. Bao, S. Li, L. Wang, Z. Liu, W. Chen, Q. Xia and G. Liang, *Tetrahedron*, 2017, **73**, 2504–2511; (*c*) J. M. Smith, J. A. Dixon, J. N. Degruyter and P. S. Baran, *J. Med. Chem.*, 2019, **62**, 2256–2264.
20 (*a*) X. Su and I. Aprahamian, *Chem. Soc. Rev.*, 2014, **43**, 1963–1981; (*b*) Q. Li, Y. Zhang, J. Lin, Y. Zou, P. Wang, Z. Qin, Y. Wang, Y. Li, Y. Zhang, C. Gao, Y. Zang, W. Hu and H. Dong, *Angew. Chem., Int. Ed.*, 2023, **62**, e202308146; (*c*) N. Eid, I. Karamé and B. Andrioletti, *Eur. J. Org. Chem.*, 2018, 5016–5022; (*d*) S. Şenkardeş, M. İhsan Han, M. Gürboğa, Ö.B Özakpinar and G. Küçükgüzel, *Med. Chem. Res.*, 2022, **31**, 368–379; (*e*) P. Patoghi, A. Sadatnabi and D. Nematollahi, *Sci. Rep.*, 2023, **13**, 17582; (*f*) S. P. Blum, T. Karakaya, D. Schollmeyer, A. Klapars and S. R. Waldvogel, *Angew. Chem., Int. Ed.*, 2021, **60**, 5056–5062; (*g*) W. Liu, J. Chen and W. Su, *Pharm. Fronts*, 2024, **6**, e355–e381.
21 J. Xu, C. Shen, X. Qin, J. Wu, P. Zhang and X. Liu, *J. Org. Chem.*, 2021, **86**, 3706–3720.
22 J. Qiao, K. Zheng, Z. Lin, H. Jin, W. Yu, C. Shen, A. Jia and Q. Zhang, *Catalysts*, 2023, **13**, 726.
23 (*a*) S. Cembellín and B. Batanero, *Chem. Rec.*, 2021, **21**, 1–20; (*b*) Y. H. Budnikova, E. L. Dolengovski, M. V. Tarasov and T. V. Gryaznova, *J. Solid State Electrochem.*, 2024, **28**, 659–676.
24 (*a*) G. M. Martins, B. Shirinfar, T. Hardwick, A. Murtaza and N. Ahmed, *Catal. Sci. Technol.*, 2019, **9**, 5868–5881; (*b*) N. Sbei, T. Hardwick and N. Ahmed, *ACS Sustainable Chem. Eng.*, 2021, **9**, 6148–6169; (*c*) Z. M. Fu, J. S. Ye and J. M. Huang, *Org. Lett.*, 2022, **24**, 5874–5878; (*d*) Z. Ma, X. Hu, Y. Li, D. Liang, Y. Dong, B. Wang and W. Li, *Org. Chem. Front.*, 2021, **8**, 2208–2214; (*e*) S. K. Mo, Q. H. Teng, Y. M. Pan and H. T. Tang, *Adv. Synth. Catal.*, 2019, **361**, 1756–1760; (*f*) Y. Shi, K. Wang, Y. Ding and Y. Xie, *Org. Biomol. Chem.*, 2022, **20**, 9362–9367; (*g*) Z. Xu, Y. Li, G. Mo, Y. Zheng, S. Zeng, P. H. Sun and Z. Ruan, *Org. Lett.*, 2020, **22**, 4016–4020.
25 Q. L. Yang, P. P. Lei, E. J. Hao, B. N. Zhang, H. H. Zhou, W. W. Li and H. M. Guo, *SynOpen*, 2023, **7**, 535–547.
26 (*a*) Z. Li, Q. Chen, P. Mayer and H. Mayr, *J. Org. Chem.*, 2017, **82**, 2011–2017; (*b*) J. L. Kice and E. Leganlc, *J. Am. Chem. Soc.*, 1973, **95**, 3912–3917.
27 (*a*) D. Kaiser, I. Klose, R. Oost, J. Neuhaus and N. Maulide, *Chem. Rev.*, 2019, **119**, 8701–8780; (*b*) A. B. Riddell, M. R. A. Smith and A. L. Schwan, *J. Sulfur Chem.*, 2022, **43**, 540–592; (*c*) M. B. Reddy and E. M. McGarrigle, *Chem. Commun.*, 2023, **59**, 7767–7770.
28 N. Tanbouza, A. Petti, M. C. Leech, L. Caron, J. M. Walsh, K. Lam and T. Ollevier, *Org. Lett.*, 2022, **24**, 4665–4669.
29 (*a*) L. Y. Lam and C. Ma, *Org. Lett.*, 2021, **23**, 6164–6168; (*b*) Y. C. Luo, X. J. Pan and G. Q. Yuan, *Tetrahedron*, 2015, **71**, 2119–2123; (*c*) X. W. Lan, N. X. Wang, C. B. Bai, W. Zhang, Y. Xing, J. L. Wen, Y. J. Wang and Y. H. Li, *Sci. Rep.*, 2015, **5**, 18391.

30 M. B. Aktekin, Z. Oksuz, B. Turkmenoglu, E. S. Istifli, M. Kuzucu and O. Algul, *Chem. Biol. Drug Des.*, 2024, **104**, e14601.
31 A. Tabassum, D. Kumari, H. B. Bhore, T. Palmo, I. Venkatesan, J. Samanta, A. K. Katare, K. Singh and Y. P. Bharitkar, *Bioorg. Chem.*, 2025, **154**, 108087.
32 R. Humphries, A. M. Bobenchik, J. A. Hindler and A. N. Schuetz, *J. Clin. Microbiol.*, 2021, **59**, e0021321.
33 R. M. Humphries, J. Ambler, S. L. Mitchell, M. Castanheira, T. Dingle, J. A. Hindler, L. Koeth and K. Sei, *J. Clin. Microbiol.*, 2018, **56**, 10–1128.
34 D. Rani, D. Kumari, A. Bhushan, V. Jamwal, B. A. Lone, G. Lakhanpal, A. Nargotra, K. Singh and P. Gupta, *J. Mol. Struct.*, 2024, **1308**, 138105.
35 P. Kaur and V. Tyagi, CCDC 2471164: Experimental Crystal Structure Determination, 2025, DOI: 10.5517/ccdc.csd.cc2nyfz1.